Catalysis Science & Technology

Direct methylation of benzene with methane over Co/MFI catalysts generated by self-dispersion of $Co(OH)_2$

Journal:	*Catalysis Science & Technology*
Manuscript ID	CY-ART-03-2023-000305.R2
Article Type:	Paper
Date Submitted by the Author:	23-Jun-2023
Complete List of Authors:	Okumura, Kazu; Kogakuin University, Tanaka, Kai; Kogakuin University - Hachioji Campus Ohtsuki, Akimichi; Kogakuin University - Hachioji Campus Iiyoshi, Hikaru; Kogakuin University - Hachioji Campus Katada, Naonobu; Tottori University, Center for Research on Green Sustainable Chemistry

Direct methylation of benzene with methane over Co/MFI catalysts generated by self-dispersion of $Co(OH)_2$

Kazu Okumura,[1] Kai Tanaka,[1] Akimichi Ohtsuki,[1] Hikaru Iiyoshi,[1] and Naonobu Katada[2]*

[1]Department of Applied Chemistry, School of Advanced Engineering, Kogakuin University, 2665-1 Nakano-machi Hachioji-city, Tokyo 192-0015, Japan

[2]Center for Research on Green Sustainable Chemistry, Tottori University, 4-101 Koyama-cho Minami, Tottori 680-8552, Japan

KEYWORDS : Cobalt, MFI, Methane, Benzene, Toluene, XAFS, Self-dispersion

ABSTRACT: Methane-benzene reaction was performed over the Co/MFI prepared with an aqueous solution of $Co(OAc)_2$ and MFI zeolite. $Co(OH)_2$ was deposited on the MFI zeolite when the $Co(OAc)_2$ solution was stirred at 343 K in the presence of MFI. Decline of h-peak in NH_3 TPD occurred during loading of Co on MFI. Further thermal treatment at 573 – 773 K caused the spontaneous formation of the atomically dispersed Co species, which was observed with Co K-

edge XAFS. The toluene formation rate of the catalyst prepared with $Co(OAc)_2$ was proportional to the Co loading and was higher than that prepared with $Co(NO_3)_2$ due to the large amount of Co supported.

1. Introduction

Methane, the main component of natural gas, is an abundant resource on earth, thus it is expected to be used not only as a fuel but also as a carbon resource. In order to use methane for non-fuel applications, it is usually converted to other molecules by C1 chemistry via synthesis gas ($CO + H_2$) obtained by steam reforming of methane with water vapor using Ni or Ru supported catalysts.[1,2] Meanwhile, if methane can be used directly as a carbon source, it is expected that a new synthetic route will be developed. The use of methane as carbon source is beneficial over conventional ones using petroleum as the carbon source for production of plastics and so on from the economical viewpoint. Various catalysts that directly utilize methane as a carbon resource have been developed including Mo-loaded MFI for the formation of benzene.[3] Among them, Co/MFI has been found to be active in the direct methylation of benzene by methane to give toluene and hydrogen.[4] The reaction proceeded exclusively when MFI zeolite was employed as the support for Co among various structure of zeolites.[5]

The conventional Co/MFI catalysts have primarily been prepared with an ion-exchange method.[6] The Co located at the α sites among three kinds of ion-exchange sites (α, β, γ) was active in the methane-benzene reaction[7] among the ion-exchange sites.[8] The adsorption energy generated at the adsorption of benzene on the Lewis acid sites of Co compensated the activation energy required for scission of the C-H bond in methane, so that reaction between methane and benzene was promoted.[7] It could be supposed that the one of the ways to improve the catalytic activity of Co/MFI zeolite is to increase the loading of Co with atomically dispersed form using ion-exchange sites of MFI. Another possible way to increase the loading of dispersed Co is to make use of the reaction between defect sits of MFI and Co. Such a method has been reported to prepare atomically dispersed species of various elements including Ti and Sb using volatile precursors.[9,10] In previous studies on Co/MFI catalysts, $Co(NO_3)_2$ has been primarily used as a precursor of Co for the preparation of Co/MFI by the above mentioned ion-exchange method under non-hydration conditions.[11] The hydrolysis of Co^{2+} ion is inhibited under the acidic condition or low temperature.[12] Other possible methods for the preparation of Co/MFI is the impregnation of $Co(NO_3)_2$ and the sublimation of volatile Co precursors.[13] In the former case, aggregated and dispersed Co oxides formed simultaneously, resulting in a heterogeneous distribution of Co sizes.[4]

In this research, we employed cobalt acetate tetrahydrate ($Co(OAc)_2 \cdot 4H_2O$) as the precursor of Co/MFI in place of $Co(NO_3)_2$ on purpose. The pH of the aqueous solution of $Co(OAc)_2$ was ca. 7.2 at 200 mmol L^{-1}. Under this condition, hydrolysis of Co^{2+} ions occurs to form $Co(OH)_2$ spontaneously at around 343 K.[14] We expected that the deposited $Co(OH)_2$ on the surface of MFI zeolites acted as the possible precursor of active Co species in methane-benzene reaction, which was generated through the reaction with defect or ion exchange sites in MFI zeolites. This is because $Co(OAc)_2$ was reported to be a promising precursor to obtain well-dispersed Co species in MFI via solid-state ion-exchange reactions.[15] MFI treated with an aqueous NaOH solution was also used as the support for Co, taking into account that treatment with an aqueous NaOH solution has been reported to change the porosity of MFI.[16]

The dispersion process of aggregated to dispersed Co species was monitored with Co K-edge X-ray absorption fine structure (XAFS), and NH_3 temperature programmed desorption (NH_3-TPD). Particularly, Co K-edge XAFS is powerful technique to obtain information on the structural and electronic state of Co center, which has been applied for the characterization of Co/zeolites so far.[17,18]

2. Experimental

2.1. Catalyst preparation

The experiment was carried out primarily using the MFI zeolite supplied by Mizusawa Chemical Co. (52A). In addition to the 52A sample, MFI, FAU, LTL, MOR, and BEA zeolites purchased from Tosoh Co. or obtained from Catalysis Society of Japan and the SiO_2 (Fuji-Silysia Co.) were employed as the support for Co as well. The composition, abbreviations of the employed zeolites are listed in Table 1. The letters "N" and "H" indicated the NH_4 and H forms of zeolites, respectively. The sample treated with an aqueous NaOH solution for zeolite is abbreviated as sample name + AT + treatment time. For example, 822N-AT6h indicated that Co was loaded on the NH_4-type 822 treated with an NaOH aqueous solution for 6 h. For the preparation of Co-loaded samples, the zeolite sample (3 g) was ion exchanged with an aqueous solution of NH_4NO_3 (200 mmol L^{-1}) at 343 K by three times for 4 h to obtain NH_4-form prior to the loading of Co. The amount of NH_4NO_3 used for each ion exchange treatment was ten times as much as the Al present in zeolites. In some sample preparations, Co was loaded on H-type zeolites. A part of the MFI samples was treated with an aqueous solution of NaOH (0.7 mol L^{-1}, 200 mL) at 313 K for 1 - 16 h. The treated samples were rinsed repeatedly with deionized water and subsequently dried in air.

The NaOH-treated MFI samples were transformed to NH_4-type after ion exchange with an NH_4NO_3 solutions (0.5 mol L^{-1}) at 343 K by three times, prior to the loading of Co. Cobalt(II) acetate tetrahydrate ($(CH_3COO)_2Co \cdot 4H_2O$) was purchased from Fujifilm Wako Pure Chemical Co. Zeolites (primarily NH_4-form) were added to the aqueous solution of $Co(OAc)_2$ (200 mL), then they were continuously stirred at 343 K for 4 h to load Co on the zeolites. $Co(OAc)_2$ solutions with different Co concentration (50 - 400 mmol L^{-1}) were used for preparation of Co/MFI. The typical concentration of $Co(OAc)_2$ was 200 mmol L^{-1}. The Co loaded samples were separated by filtration, rinsed repeatedly with deionized water, and dried in an oven kept at 373 K. The loading of Co on silica was carried out in the same manner as for the preparation of Co/zeolites.

2.2. Sample characterization

Co K-edge XAFS data of the $Co(OAc)_2$-loaded supports were collected using synchrotron radiation. The data were recorded at the BL-9C beamline with the approval of the Photon Factory of the High Energy Accelerator Research Organization (KEK-PF). Proposal numbers were 2020G621 and 2022G581. The samples pressed into a wafer form (one pellet) were subjected to the XAFS measurement under ambient conditions. The data was obtained in a quick scan mode

within 5 min using a Si (111) monochromator in the transmission mode. The ion chambers for the detection of primary (I_0, 100% N_2) and transmitted (15% Ar with the balance N_2) were used for data acquisition. The beam size at the sample position was 1.0 mm (horizontal) × 1.0 mm (vertical). The Co K-edge extended X-ray absorption fine structure (EXAFS) was analyzed by extracting oscillations using a spline smoothing method. The Fourier transform (FT) of the k^3-weighted EXAFS oscillations and $k^3\chi(k)$ from k-space to r-space was conducted in the range of 3 – 13 $Å^{-1}$ for curve-fitting analysis. The EXAFS data were analyzed using the REX software (Rigaku Co.). The parameters for the analysis of the Co–O and Co-Co bonds were extracted from Co K-edge EXAFS of CoO and Co foil, respectively. For the analysis of the Co−Si bond, parameters were obtained using the FEFF8.0 code.[19] In addition to the ex-situ conditions, operando XAFS measurement was carried out at BL-9C of KEK-PF. For this purpose, a wafer sample (40 mg, 10 mm-ϕ) was mounted in a stainless-steel cross-shaped cell. XAFS and IR measurements were performed using crossed X-ray and Infrared (IR) beams at the sample position (Figure S1). The sample pellet was placed on the optical path at an angle of 45° to the X-ray and IR. Data of the Co K-edge XAFS was obtained under flowing N_2 (30 mL min^{-1}) while raising the temperature (heating rate: 10 K min^{-1}).

Co loadings were measured with the atomic absorption (AA) instrument AA-6200 (Shimadzu Co.). The sample was prepared after dissolving Co/MFI with an aqueous solution of HF and subsequently with conc. H_2SO_4, followed by evaporation. The residue dissolved with hydrochloric acid was subjected to the AA measurements for quantitative analysis of Co. Data of the temperature programmed desorption (TPD) of ammonia was obtained with a BELCAT II equipment (Microtrac Bel Co.). The sample was treated at 773 K in an N_2 flow prior to the measurement. Then ammonia (5%) diluted with N_2 was equilibrated with the pretreated sample (0.1 g) at 373 K. The TPD data were collected with the temperature ramping rate of 10 K min^{-1}. The carrier gas (He) flow rate was 30 mL min^{-1}. A mass spectrometer (BELMASS, Microtrac Bel Co.) was used to measure the desorbed NH_3. In the measurement, m/z =16 was monitored to analyze the desorbed NH_3. X-ray diffraction (XRD) patterns of the powder samples were obtained using a MiniFlex X-ray diffractometer (Rigaku Co.) with Cu $K\alpha$ radiation in the 2θ range from 3 to 40˚ with 10°/min scanning speed. N_2 adsorption isotherms were recorded on the BELSORP-mini-X (Microtrac Bel Co.) instrument. The samples were dehydrated in vacuum at 413 K in advance. Transmission electron microscopy (TEM) images were obtained using a JEOL-JEM-2100 microscope. For the preparation of the sample, an ethanol suspension of the Co/MFI was

dropped onto Cu grids coated with a C-coated porous thin membrane (NEM, Japan) and dried. TEM observations were performed at an operating voltage of 200 kV. Field emission scanning electron microscopy (FE-SEM) images were taken with a JEOL JSM-6701F microscope with an acceleration voltage of 5 kV.

2.3. Catalytic reaction

Catalytic reaction between methane and benzene was performed using a fixed-bed flow reactor. The prepared catalyst was mounted in a reaction tube filled with quartz wool, which was placed at the bottom of the powder catalyst. The catalyst (0.30 g) was pretreated at 823 K in an N_2 flow for 1 h prior to the reaction. Neat methane gas (99.995%) was passed through a bubbler containing liquid benzene (Fuji Film Wako Pure Chemical Industries) kept at 273 K with a flow rate of 30 mL min^{-1}. The gas mixture was reacted with the pretreated Co/MFI catalyst at 823 K. The ratio of methane to benzene was 29 : 1. The effluent gas was analyzed with an on-line FID type gas chromatography (Shimadzu, GC-2014) equipped with a capillary column (GL Sciences Inc., InertCap 1). Toluene formation rate was calculated based on the benzene feed flow rate (2.7 mmol h^{-1}).

3. Results and Discussion

3.1. Operando Co K-edge XAFS and IR studies

First, the local structure of the Co/MFI(52N) was analyzed with Co K-edge XAFS for as prepared and the samples pretreated in an N_2 flow. Figure 1(a) shows the Co K-edge X-ray absorption near edge structure (XANES) of the sample in which Co was loaded on MFI using $Co(OAc)_2$ as a precursor (as prepared) and reference compounds. The XANES of the as prepared Co/MFI sample was close to that of $Co(OH)_2$, indicating that the $Co(OAc)_2$ was hydrated to give $Co(OH)_2$ during heat treatment of a $Co(OAc)_2$ solution in the presence of MFI at 343 K. As shown in Figure 1(b), the Co K-edge X-ray absorption fine structure (EXAFS) of the Co/MFI samples was also close to that of $Co(OH)_2$. The corresponding $k^3\chi(k)$ data was displayed in Figure S2. That is to say, two peaks assignable to the Co-O and Co-(O)-Co bonds appeared at 1.7 and 2.8 Å (phase shift uncorrected) in the EXAFS Fourier transform (EXAFS-FT), respectively. It has been reported that the dehydration of $Co(OAc)_2$ occurred at high pH or heat treatment around neutral conditions.[14] Therefore, it was likely that hydration of $Co(OAc)_2$ proceeded during the preparation of Co/MFI to form $Co(OH)_2$ and acetic acid. The loading of Co in Co/MFI (52N) increased gradually with increasing concentration of $Co(OAc)_2$ measured by AA (Figure 2(a)). At the same

time, the Al content of MFI decreased and the Co loading increased (Figure 2(b)). However, no shift of the diffraction in XRD pattern was observed in the two 2θ regions before and after the loading of Co on MFI (Figure S3) when the 2θ angle was corrected with the MgO as an internal standard. The fact indicated that the dealumination of framework Al hardly occurred. Instead, considering that MFI(52A) contains large amount of extra framework Al (0.37 mmol g^{-1}), which was larger than that of framework Al (0.25 mmol g^{-1}), probably the extra framework Al species were removed during Co loading. The Co/Al ratio of the Co/MFI exceeded 0.5 or 1.0 in many samples, suggesting that $Co(OH)_2$ deposition occurred independently of the Al sites in the MFI (Figure S4).

The loading of Co on MFI(52N) was 0.18 mmol g^{-1} when a 100 mmol L^{-1} $Co(NO_3)_2$ aqueous solution was used as the precursor for Co under acidic (non hydration) conditions, which has been generally employed as the Co precursor. The loaded amount of Co (0.18 mmol g^{-1}) was comparable to that of ion-exchangeable sites of 52N (0.25 mmol g^{-1}) assuming that the ion-exchange occurred between NH_4^+ and $Co(OAc)_2$ or $Co(OH)_2$ to form $Co(OH)^+$ species. On the other hand, the Co loading increased to 0.48 mmol g^{-1} when a100 mmol L^{-1} $Co(OAc)_2$ aqueous solution was used for the Co/MFI preparation, which exceeded the ion exchange capacity of 52N

(0.25 mmol g^{-1}). The higher Co loading with the use of $Co(OAc)_2$ precursor suggested that formation of dispersed Co occurred through not only the ion exchange but also the reaction with defect sites with $Co(OH)_2$.

Then the Co K-edge XAFS data was collected in an N_2 flow while temperature was heated from 303 to 823 K in order to monitor the local structure of Co species accompanied by heat treatments. The XANES data obtained at in situ condition every 50 K are displayed in Figure 3(a). A gradual decrease in the white line intensity of the Co K-edge XANES was observed up to 823 K as plotted in Figure 3(b). The changes up to 573 K observed in XANES may be due to the dehydration of $Co(OH)_2$ to form CoO, consistent with the literature.[20] The change occurred progressively in the temperature range between 303 K and 823 K, as shown in Figure S5; fitting the intermediate-stage XANES with a linear combination of the spectra obtained at room temperature and 823 K showed that the former component continuously decreased and the latter increased instead with increasing temperature. At the same time, intensity of the pre-edge peak (7702 eV) increased with increasing temperature up to 823 K. This pre-edge peak is attributed to the 1s to 3d transition, which is normally dipole forbidden but allowed when the metal has tetrahedral coordination due to the mixing with p-chracter.[21,22] Therefore, the change may be due

to the transformation of the local structure from 6- to 4-coordinated Co center. This could be caused by the removal of water molecules coordinated to the Co centers during the heat treatment and subsequent reaction of Co with OH groups or acid sites in MFI.

Figure 4(a) shows the Co K-edge EXAFS Fourier transform (FT) of the sample in which Co was loaded on MFI (52N) using $Co(OAc)_2$ as a precursor measured during heat treatment. Raw XAFS and $k^3\chi(k)$ data are displayed in Figure S6(a) and (b), respectively. Co loading of the measured sample was 0.5 mmol g^{-1}. When these samples were heated from 573 to 823 K, intensity of the Co-O-Co bond (2.8 Å) decreased while the Co-O peak remained almost intact. In the IR spectra measured at the same time, the intensity of isolated hydroxyl groups appearing at 3730 cm^{-1} remained unchanged, while the NH_4^+ stretching vibration peak at 3370 cm^{-1} decreased,[23] indicating the decomposition of NH_4^+ progressed during heat treatment. The intensity of the acidic hydroxyl group at 3590 cm^{-1} tended to decrease with increasing temperature, suggesting ion exchange between H^+ or NH_4^+ occurred with Co^{2+}, but at the same time, the formation of acidic hydroxyl groups progressed as a result of the decomposition of NH_4^+ (Figure S7). The EXAFS oscillation is greatly reducing as the temperature rises because the Debye-Waller factor increases at high temperature. To prevent this temperature effect, XAFS data of the heat-treated samples

were collected at 298 K (Figure 4(b)). The corresponding $k^3\chi(k)$ data is displayed in Figure S8(a). A significant decrease in the intensity of the second peak appearing at 2.8 Å (phase shift uncorrected) was observed in the temperature range of 573–773 K. A similar change was observed in the Co/MFI containing lower Co loading (0.3 mmol g^{-1}, Figure S8(b), (c)). The EXAFS of the as prepared Co/MFI sample was successfully fitted after assuming Co-O and Co-(O)-Co bonds, while that of 773 K-treated one was fitted after assuming Co-O and Co-(O)-Si bonds as listed in Table 2 and shown in Figure S9. The change observed after treatment at 773 K meant that the aggregated $Co(OH)_2$ undergo self-dispersion through the interaction with MFI zeolite. Such dispersion was also found in Pd on MFI or MOR zeolites.[24] Another examples are the formation and segregation of Ir, Pt-MgO solid solutions observed in the temperature range between 773 and 1273 K.[25,26] A similar change (decline) of Co-(O)-Co bond appeared at 2.8 Å was observed in Co/SiO_2 (Co loading: 0.5 mmol g^{-1}) as displayed in the EXAFS-FT (Figure S10(b)); the peak was significantly reduced after the treatment at 773 K. This structural change suggested that the self-dispersion of Co occurred on Co/SiO_2, similar to the case of Co/MFI.

3.2. NH_3 TPD and XRD patterns

Figure 5 shows the NH_3 TPD profile of Co/MFI(52N) with different Co loading. Intensity of the h-peak appeared around 730 K was much lower than that of unloaded MFI(52N), while change in the l-peak at ca. 500 K was small. The NH_3 TPD profile did not change depending on the Co loading. The decline of the h-peak (730 K) observed after the loading of Co might be caused by the ion exchange of H^+ with Co^{2+}.

NH_3 TPD profiles of employed MFI zeolites (NH_4^+ form) and those of untreated 822N and those treated with an aqueous solution of NaOH, followed by treated with NH_4NO_3 solution at 343 K are displayed in Figure S11(a) and (b), respectively. In the latter case, intensity of the h-peak decreased in the MFI treated with an NaOH solution for 16 h. This means that the number of Al atoms in the MFI framework decreased after NaOH treatment. In agreement with this, the XRD patterns revealed that partial collapse of the MFI crystals occurred after treatment with NaOH for 16 h as will be shown later. In general, the treatment of zeolite with NaOH solution resulted in the preferential dissolution of Si.[27] Consistent with this, the total Al concentration in the MFI increased with treatment time, as shown in Figure S12. As for Al distribution, amount of framework Al decreased, while that of extra-framework Al increased with increasing treatment time with an aqueous solution of NaOH (Table S1).

XRD diffraction patterns of the as prepared Co/MFI(52N) and those treated at 773 K as well as unloaded MFI(52N) are displayed in Figure 6(a) and (b), respectively. For Co-loaded MFI(52N), no diffraction other than those ascribed to the MFI zeolite was observed after the loading of $Co(OAc)_2$ (Figure 6(a)), while the Co-(O)-Co bond appeared at 2.8 Å in the Co K-edge EXAFS already shown in Figure 4(a, b), indicating that Co existed on the MFI in an aggregated form. The contradictory data suggested that the crystallite size of $Co(OH)_2$ was less than several nm. In agreement the observation, no clear aggregate of $Co(OH)_2$ was observed in the TEM image as will be noted later. Meanwhile, the overall intensity of the diffraction peaks decreased after the loading of Co. The extent was enhanced by increasing the Co loadings. The feature did not change after the thermal treatment in N_2 at 773 K (Figure 6(b)).

XRD patterns of the as received MFI(822N) and those treated with NaOH are displayed in Figure S13. The overall intensity of the diffraction declined accompanied by increase in the concentration of the NaOH solutions, suggesting the partial collapse of MFI framework took place during the treatment with the NaOH solution and the extent of which was enhanced as increase in the concentration of the NaOH solution.

3.3. N_2 adsorption isotherms, SEM and TEM images

The N_2 adsorption isotherms of the unloaded MFI(52N) and Co-loaded ones are displayed in Figure S14(a). The isotherms of the Co/MFI (0.4 mmol g^{-1}) was identical to that of Co-unloaded one. The specific surface areas derived from the isotherm are plotted as a function of Co loadings in Figure 7. A gradual decrease in surface area was observed with increasing Co loading between 0.4 and 0.7 mmol g^{-1}. The tendency was consistent with the XRD pattern; a decrease in diffraction intensity was observed with increasing Co loading (Figure 6).

FE-SEM images of the representative MFI(822N, 840N, and 52N) employed as the support for Co are displayed in Figure 8. The average crystal size of 840N was ca. several μm (Figure 8(b)). The large crystal size agreed with the appearance of N_2 adsorption isotherm in that the isotherm of the samples was assignable to type I as shown in Figure S14(b). The size of the primary particle of 52N, and 822N, was much smaller than that of 840N; in the former cases, the size was ca. 50 nm. Consistent with this SEM figure, a progressive increase in the nitrogen adsorption isotherm curve was observed at pressures above $p/p_0 = 0.01$ (Figure 14(b)).

No difference was found between TEM images of Co/MFI(52N, as prepared sample and those thermally treated at 823 K) and Co-unloaded MFI(52N) as shown in Figure S15, suggesting that the degree of the aggregation of the deposited $Co(OH)_2$ was limited in the preparation step. The fact was consistent with the XRD patterns in that no diffraction assignable to the crystalline $Co(OH)_2$ was observed (Figure 6(a)).

3.4. Catalytic reaction

Figure 9 shows the time-course change in the rate of toluene formation over Co loaded on different kinds of zeolites. A slight decrease in formation rate was observed in the highly active samples of Co/MFI, but the activity of the catalyst was relatively stable. It can be seen from the Figure 9 (a) and (b) that the formation rate was dependent on the kinds of employed MFI zeolites. Co loaded on zeolites other than MFI was almost inactive in the reaction (Figure 9(c)). The specific high activity of Co supported on MFI was also found with the catalyst using $Co(NO_3)_2$ as the precursor.[4] The H^+- and Na^+-MFI have strong Brønsted and Lewis acid character, respectively.[28,29] Therefore, we speculate that the strong adsorption of benzene on the Lewis sites of Co^{2+} promoted

the reaction with methane, the presence of which was confirmed with IR spectra of adsorbed NH_3.[7] Rate of toluene formation at 3 h of the time on stream from the beginning of the reaction in Co/MFI are plotted as a function of Co loading in Figure 10(a). The toluene formation rate was almost proportional to the loading of Co up to 1.0 mmol g^{-1} except for the Co/MFI(822N-AT16h), in which excessive Co was loaded on the MFI support (Co loading: 1.5 mmol g^{-1}). Since the formation rate of H-type MFI and Co-loaded samples of NH_4-type MFI follow the same line, cationic species of MFI during catalyst preparation had no influence on the catalytic activity of Co. The linear relationship indicated that the catalytic activity of Co/MFI depended only on Co loading. The highest toluene formation rate (11.3 μmol $gcat^{-1}$ min^{-1}) was higher than that (6.2 μmol $gcat^{-1}$ min^{-1}) of Co/MFI(52N, Co loading: 0.34 mmol g^{-1}) prepared using $Co(NO_3)_2$ as the Co precursor with an impregnation method. Turnover frequency (TOF) value of Co/MFI prepared with $Co(OAc)_2$ distributed in the range of 0.58 – 0.85 h^{-1} with the exception of several samples (Figure 10(b)).

4. Conclusions

In this study, we found that $Co(OH)_2$ precipitated on MFI when $Co(OAc)_2$ was used as a precursor for Co/MFI. Further heat treatment led to self-dispersion of Co^{2+} species between 573 and 773 K. The toluene formation rate in the Co/MFI-catalyzed methane–benzene reaction was proportional to Co loading up to 1.0 mmol g^{-1}, suggesting that the catalytic activity was simply determined by the Co loading. Traditionally, atomically dispersed active species using zeolite defect sites have been prepared using volatile precursors. However, as found here, more readily available metal salts ($Co(OAc)_2 \cdot 4H_2O$) can be another precursors by making use of the self-dispersion of active species.

ACKNOWLEDGMENTS

This study was supported by JST CREST Grant Number JPMJCR17P1, Japan. Technical support for operando IR-XAFS measurements was provided by Dr. K. K. Bando (AIST).

References

1. J. P. Van Hook, *Catalysis Reviews—Science and Engineering*, 1980, **21**, 1-51.

2. Y. Zhao, H. Sohn, B. Hu, J. Niklas, O. G. Poluektov, J. Tian, M. Delferro and A. S. Hock, *ACS Omega*, 2018, **3**, 11117-11127.

3. T. Armaroli, M. Bevilacqua, M. Trombetta, F. Milella, A. d. G. Alejandre, J. Ramírez, B. Notari, R. J. Willey and G. Busca, *Appl. Catal. A*, 2001, **216**, 59-71.

4. K. Nakamura, A. Okuda, K. Ohta, H. Matsubara, K. Okumura, K. Yamamoto, R. Itagaki, S. Suganuma, E. Tsuji and N. Katada, *ChemCatChem*, 2018, **10**, 3806-3812.

5. K. Nakamura, K. Okumura, E. Tsuji, S. Suganuma and N. Katada, *ChemCatChem*, 2020, **12**, 2333-2340.

6. Y. Yan, X. Zhang, J. Wei, M. Chen, J. Bi and Y. Bao, *ACS Omega*, 2022, **7**, 17811-17821.

7. H. Matsubara, K. Yamamoto, E. Tsuji, K. Okumura, K. Nakamura, S. Suganuma and N. Katada, *Micropor. Mesopor. Mater.*, 2021, **310**, 110649.

8. J. Dědeček, D. Kaucký and B. Wichterlová, *Micropor. Mesopor. Mater.*, 2000, **35**, 483-494.

9. P. Wu, T. Komatsu and T. Yashima, *J. Phys. Chem.*, 1996, **100**, 10316-10322.

10. K. Yamagishi, S. Namba and T. Yashima, *Stud. Surf. Sci. Catal.*, 1989, **49**, 459-467.

11. R. Da Cruz, A. Mascarenhas and H. M. C. Andrade, *Appl. Catal. B*, 1998, **18**, 223-231.

12. Y. Kishi, S. Shigemi, S. Doihara, M. Mostafa and K. Wase, *Hydrometallurgy*, 1998, **47**, 325-338.

13. X. Wang, H. Chen and W. Sachtler, *Appl. Catal. B*, 2001, **29**, 47-60.

14. M. Eguchi and A. Yazawa, *Nippon Kogyo Kaishi*, 1975, **91**, 39-44 (in Japanese).

15. M. Mhamdi, S. Khaddar-Zine and A. Ghorbel, *Appl. Catal. A*, 2009, **357**, 42-50.

16. M. S. Holm, S. Svelle, F. Joensen, P. Beato, C. H. Christensen, S. Bordiga and M. Bjørgen, *Appl. Catal. A*, 2009, **356**, 23-30.

17. L. Drozdová, R. Prins, J. Dědeček, Z. Sobalík and B. Wichterlová, *J. Phys. Chem. B*, 2002, **106**, 2240-2248.

18. H. Matsubara, E. Tsuji, Y. Moriwaki, K. Okumura, K. Yamamoto, K. Nakamura, S. Suganuma and N. Katada, *Catal. Lett.*, 2019, **149**, 2627-2635.

19. A. L. Ankudinov, B. Ravel, J. Rehr and S. Conradson, *Phys. Rev. B*, 1998, **58**, 7565-7576.

20. T. Jiang and D. Ellis, *J. Mater. Res.*, 1996, **11**, 2242-2256.

21. S. DeBeer George, P. Brant and E. I. Solomon, *J. Am. Chem. Soc.*, 2005, **127**, 667-674.

22. M. D. Wirt, I. Sagi, E. Chen, S. M. Frisbie, R. Lee and M. R. Chance, *J. Am. Chem. Soc.*, 1991, **113**, 5299-5304.

23. A. Zecchina, L. Marchese, S. Bordiga, C. Paze and E. Gianotti, *J. Phys. Chem. B*, 1997, **101**, 10128-10135.

24. K. Okumura, J. Amano, N. Yasunobu and M. Niwa, *J. Phys. Chem. B*, 2000, **104**, 1050-1057.

25. K. Okumura, H. Hoshi, H. Iiyoshi and H. Takaba, *ACS Omega*, 2022, **7**, 27458-27468.

26. K. Okumura, H. Hoshi and H. Iiyoshi, *Catal. Surv. Asia*, 2023, **27**, 95-106.

27. S. Abello, A. Bonilla and J. Perez-Ramirez, *Appl. Catal. A*, 2009, **364**, 191-198.

28. N. Katada, H. Igi, J.-H. Kim and M. Niwa, *J. Phys. Chem. B*, 1997, **101**, 5969-5977.

29. R. Yoshimoto, K. Hara, K. Okumura, N. Katada and M. Niwa, *J. Phys. Chem. C*, 2007, **111**, 1474-1479.

Table 1. Zeolites and silica samples employed as the support for Co

Sample name	Structure	Abbreviation	Supplier	Cation type	Si/Al_2
HSZ-820NHA	MFI	820	Tosoh Co.	NH_4^+	23
HSZ-822HOA	MFI	822	Tosoh Co.	H^+	24
HSZ-840HOA	MFI	840	Tosoh Co.	H^+	40
HSZ-860HOA	MFI	860	Tosoh Co.	H^+	72
HSZ-891HOA	MFI	891	Tosoh Co.	H^+	1500
52A	MFI	52	Mizusawa Chemical Co.	Na^+,H^+	52
JRC-Z5-90NA	MFI	90	Catalysis Society of Japan	Na^+	90
HSZ-360UHA	FAU	360	Tosoh Co.	H^+	15
HSZ-500KOA	LTL	500	Tosoh Co.	K^+	6.1
HSZ-640HOA	MOR	640	Tosoh Co.	H^+	380
HSZ-930NHA	BEA	930	Tosoh Co.	NH_4^+	27
Q3	SiO_2	SiO_2	Fuji-Silysia Co.	-	-

Table 2. Curve fitting analysis of the Co K-edge EXAFS data measured at 298 K for Co/MFI(52N, Co loading: 0.5 mmol g^{-1})

Sample	Scatterer	CN[a]	R / Å[b]	ΔE_0/ eV[c]	DW/ Å[d]	R_f / %[e]
as prepared Co/MFI(52N)	O	5.2±1.1	2.07±0.02	1±3	0.084±0.027	0.6
	Co	5.1±1.3	3.14±0.02	4±2	0.086±0.023	
Co/MFI(52N) treated at 773 K	O	4.9±0.8	2.08±0.01	4±2	0.087±0.020	2.3
	Si	2.0±1.0	3.27±0.03	-4±5	0.062±0.067	
$Co(OH)_2$[f]	O	(6)	(2.13)			
	Co	(6)	(3.20)			

[a]coordination number, [b]bond distance, [c]difference in the origin of photoelectron energy between the reference and the sample, [d]Debye-Waller factor, [e]residual factor, [f]data of X-ray crystallography. Fourier transform range: 3 – 13 $Å^{-1}$. Fourier filtering range: 1 - 3 Å.

Figure Captions

Figure 1. Co K-edge (a) XANES, and (b) EXAFS FT of Co/MFI(52N) (Co: 0.5 mmol g^{-1}) and reference compounds measured at 298 K. Fourier transform range: 3 – 13 $Å^{-1}$.

Figure 2. (a) Relationship between Co loading of Co/MFI (52N) and concentration of $Co(OAc)_2$. (b) Relationship between Al concentration and Co loading of Co/MFI(52N).

Figure 3. (a) Co K-edge XANES of Co/MFI(52N) (Co: 0.5 mmol g^{-1}) measured under N_2 flow from 303 to 823 K measured under in situ conditions. (b) white line area in Co K-edge XANES of Co/MFI(52N) plotted as a function of the treatment temperature.

Figure 4. Co K-edge EXAFS FT of Co/MFI(52N) (Co: 0.5 mmol g^{-1}) (a) measured under N_2 flow from 323 to 823 K under in situ condition, the as prepared sample and (b) measured under ambient condition.

Figure 5. NH_3 TPD profile of unloaded MFI(52N) and Co/MFI(52N). The samples were treated in an N_2 flow at 773 K prior to the TPD measurement. The numbers indicate the loading of Co (mmol g^{-1}).

Figure 6. XRD patters of Co-unloaded MFI and Co/MFI. (a) as prepared, and (b) 773 K-treated samples. The numbers indicate the Co loading (mmol g^{-1}).

Figure 7. Specific surface area plotted as a function of Co loadings of Co/MFI(52N).

Figure 8. FE-SEM images of (a) 52N, (b) 840N, (c) 822N, and (d) 822N-AT16h.

Figure 9. Time course change of the toluene formation rate over Co loaded on different kinds of zeolite supports: (a) NH_4-form MFI, (b) H-form MFI, and (c) zeolites other than MFI. The Co/MFI catalysts were prepared using a 200 mmol L^{-1} $Co(OAc)_2$ solution at 343 K for 4 h. The numbers in the parenthesis indicate the loading of Co (mmol g^{-1}).

Figure 10. (a) Toluene formation rate at 3 h of the time on stream plotted as a function of Co loading for Co/MFI catalysts. The Co/MFI catalysts were prepared using a $Co(OAc)_2$ solution (200 mmol L^{-1}) at 343 K for 4 h. The linear plot was made without the addition of the data of 822N-AT16h. (b) TOF (h^{-1}) plotted as a function of Co loading. The TOF values were calculated based on the toluene formation rate at 3 h of the time on stream from the beginning of the reaction and the Co loading.

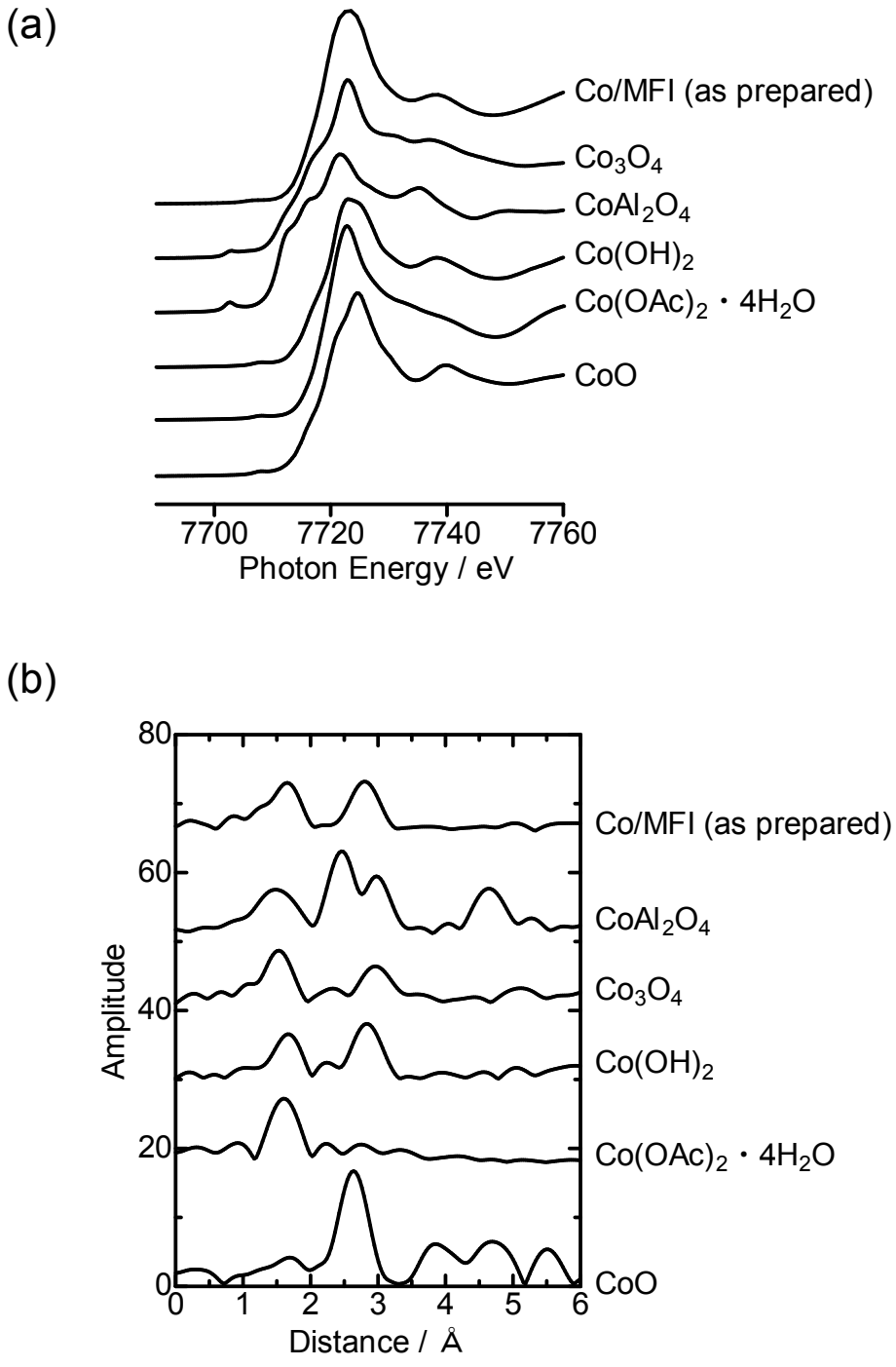
(a)
Co/MFI (as prepared)
Co_3O_4
$CoAl_2O_4$
$Co(OH)_2$
$Co(OAc)_2 \cdot 4H_2O$
CoO
7700
7720
7740
7760
Photon Energy / eV
(b)
80
60
40
20
0
Amplitude
Co/MFI (as prepared)
$CoAl_2O_4$
Co_3O_4
$Co(OH)_2$
$Co(OAc)_2 \cdot 4H_2O$
CoO
0 1 2 3 4 5 6
Distance / Å

Figure 1

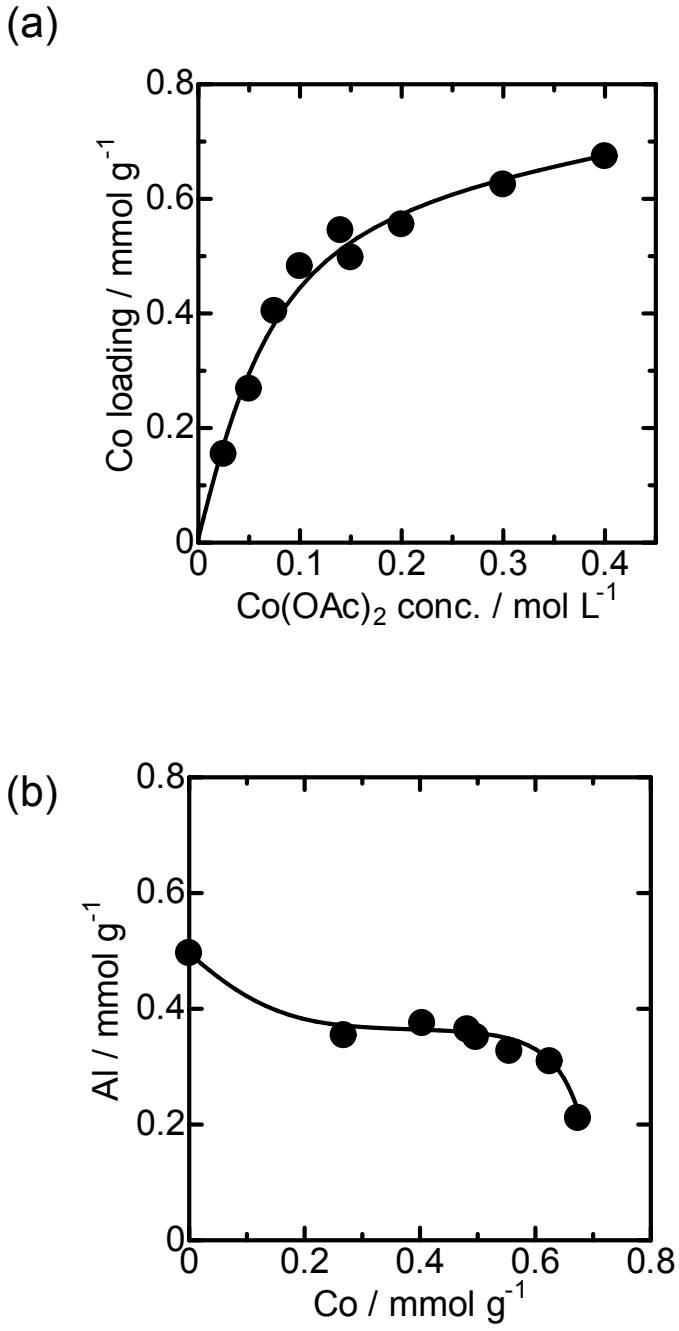
(a)
Co loading / mmol g-1
0
0.2
0.4
0.6
0.8
0
0.1
0.2
0.3
0.4
Co(OAc)2 conc. / mol L-1
(b)
Al / mmol g-1
0
0.2
0.4
0.6
0.8
0
0.2
0.4
0.6
0.8
Co / mmol g-1

Figure 2

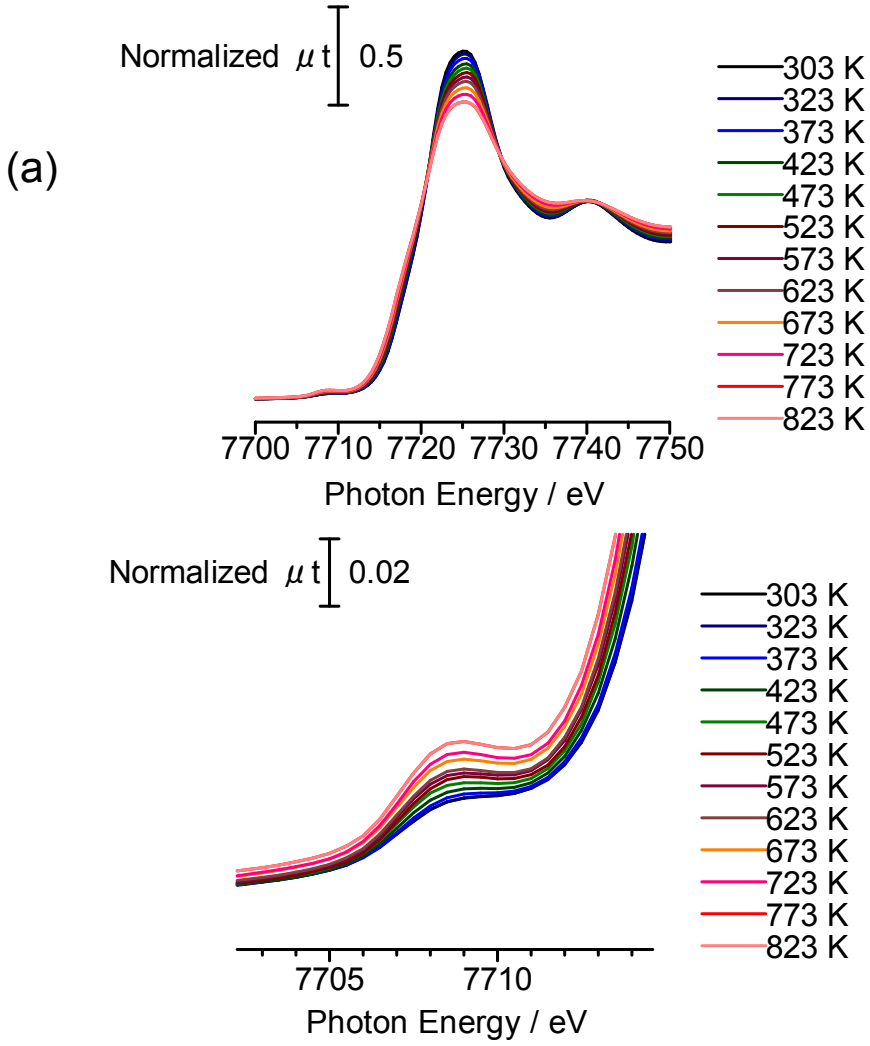
(a)
Normalized μt 0.5
303 K
323 K
373 K
423 K
473 K
523 K
573 K
623 K
673 K
723 K
773 K
823 K
7700 7710 7720 7730 7740 7750
Photon Energy / eV
Normalized μt 0.02
303 K
323 K
373 K
423 K
473 K
523 K
573 K
623 K
673 K
723 K
773 K
823 K
7705 7710
Photon Energy / eV

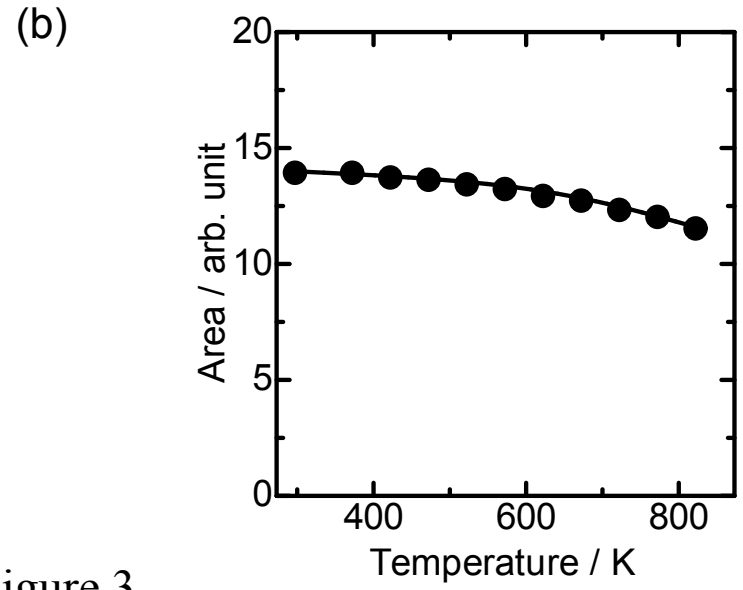
(b)
Area / arb. unit
0 5 10 15 20
400 600 800
Temperature / K

Figure 3

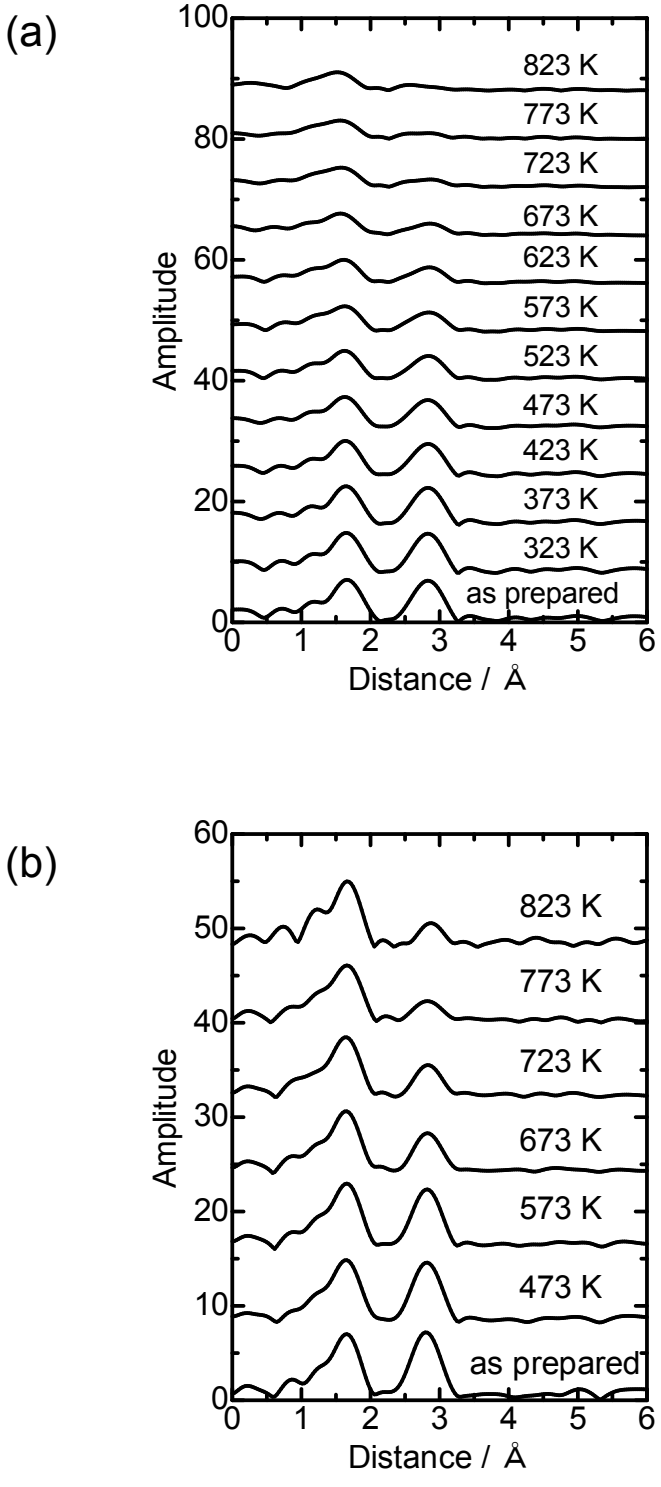
(a)
Amplitude
Distance / Å
823 K
773 K
723 K
673 K
623 K
573 K
523 K
473 K
423 K
373 K
323 K
as prepared
(b)
Amplitude
Distance / Å
823 K
773 K
723 K
673 K
573 K
473 K
as prepared

Figure 4

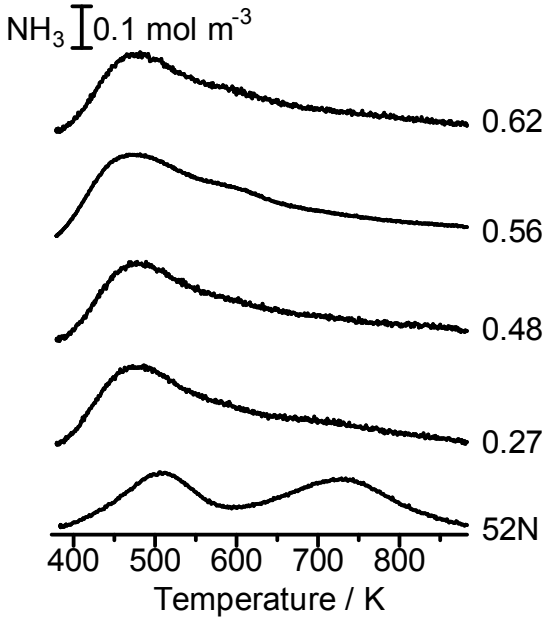
NH3
0.1 mol m-3
0.62
0.56
0.48
0.27
52N
400
500
600
700
800
Temperature / K

Figure 5

(a)

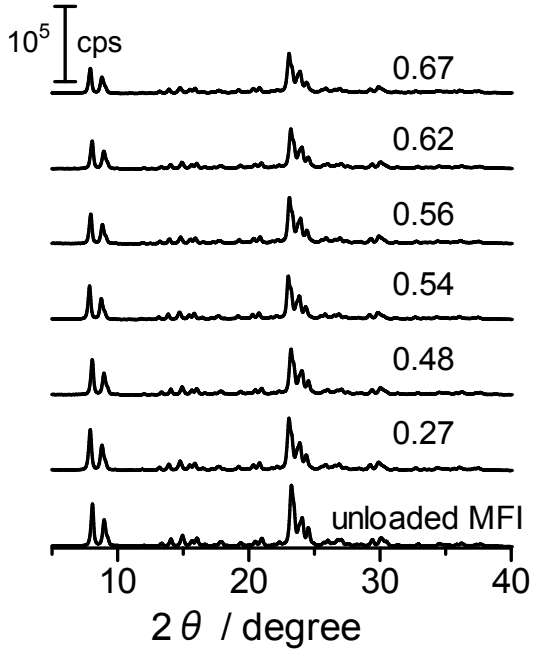
10^5 cps
0.67
0.62
0.56
0.54
0.48
0.27
unloaded MFI
10
20
30
40
2θ / degree

(b)

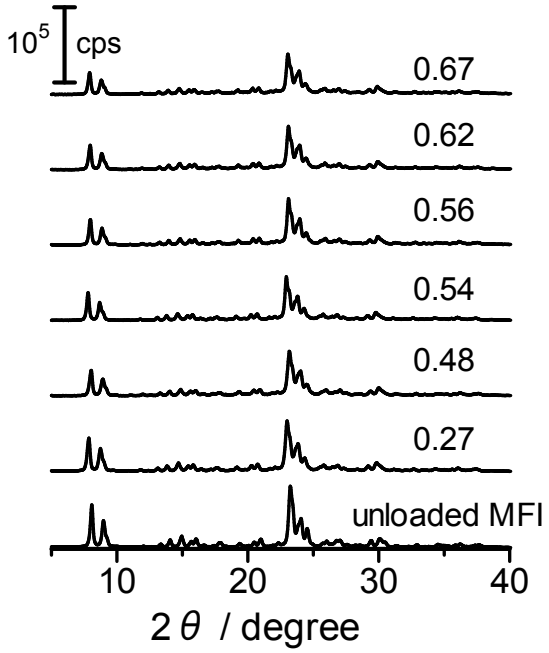
10^5 cps
0.67
0.62
0.56
0.54
0.48
0.27
unloaded MFI
10
20
30
40
2θ / degree

Figure 6

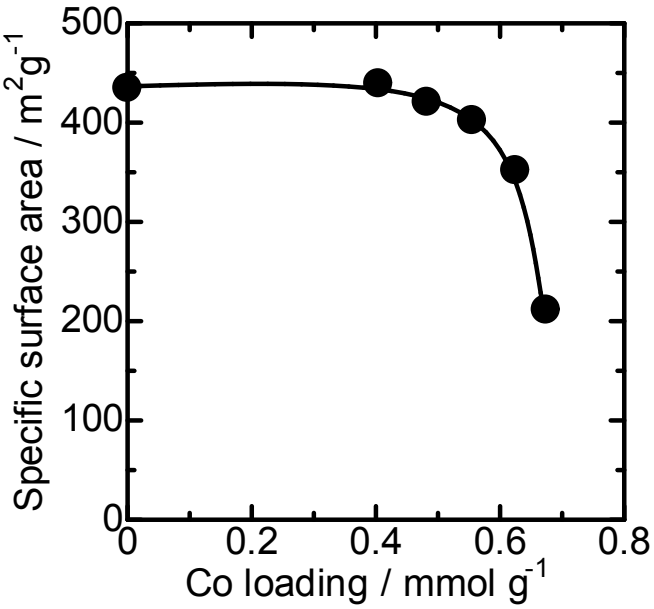
Specific surface area / m2g-1
500
400
300
200
100
0
0
0.2
0.4
0.6
0.8
Co loading / mmol g-1

Figure 7

(a)

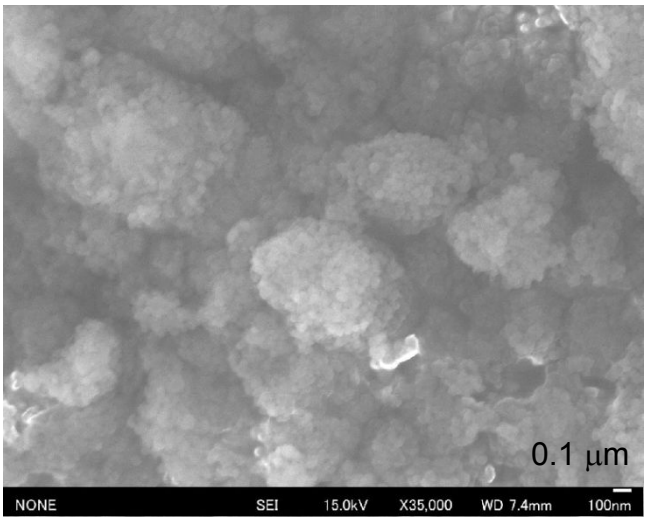

(b)

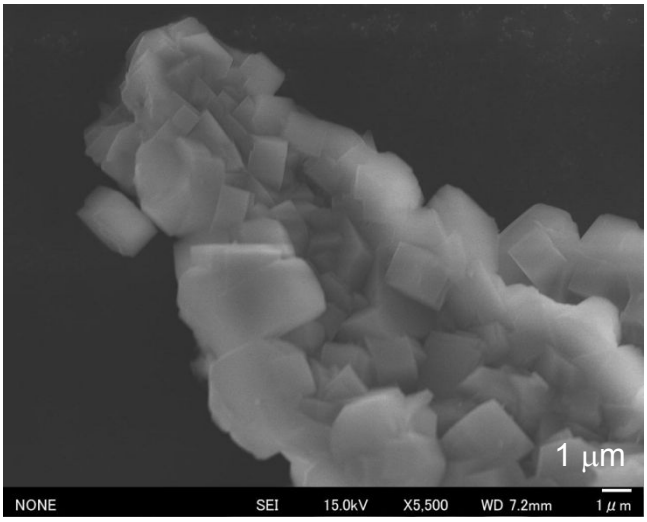

(c)

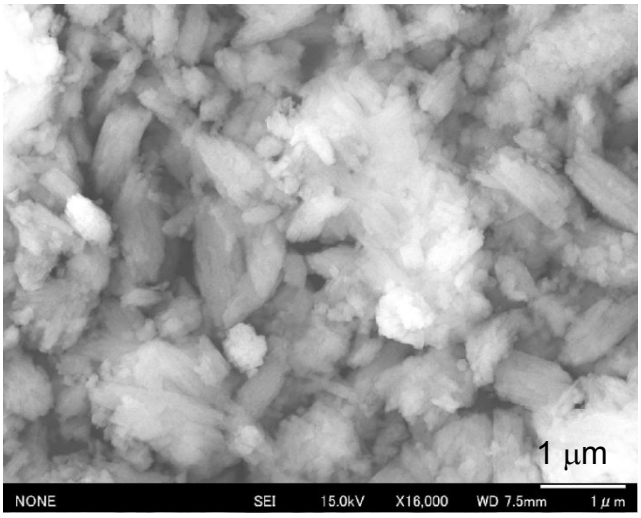

(d)

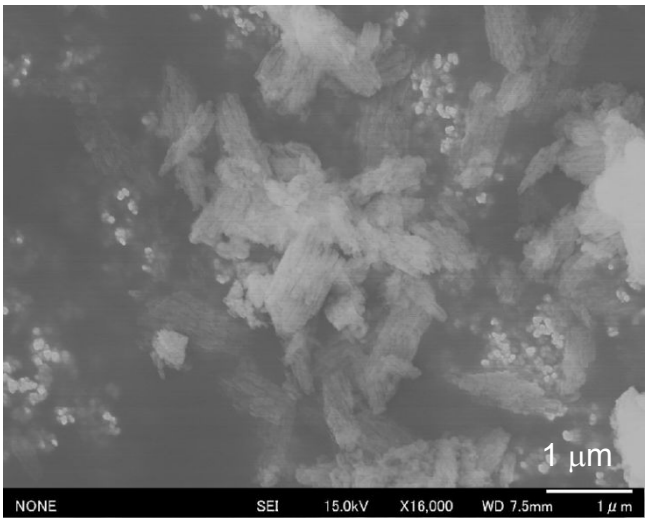

Figure 8

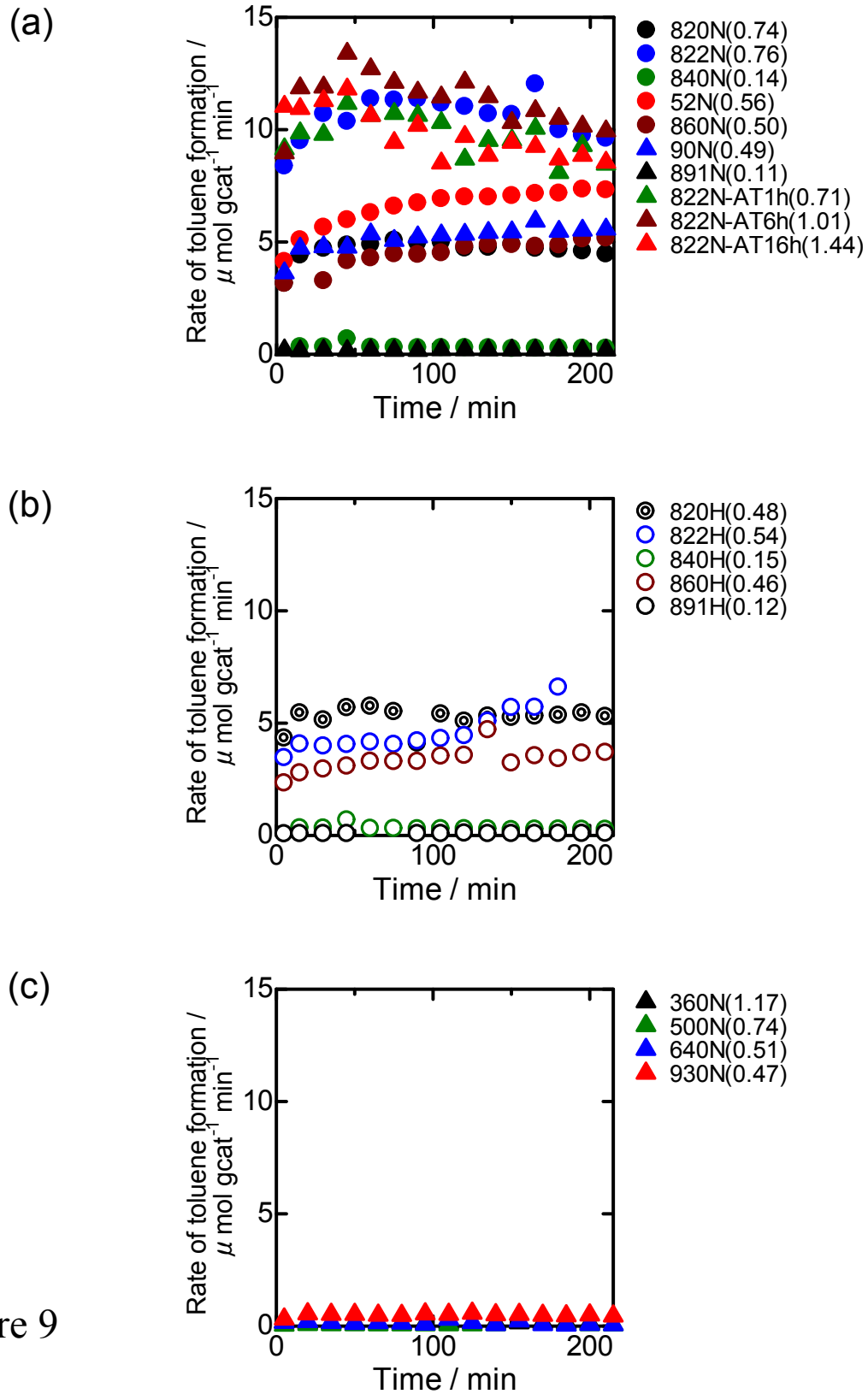
(a)
Rate of toluene formation / μ mol gcat-1 min-1
Time / min
820N(0.74)
822N(0.76)
840N(0.14)
52N(0.56)
860N(0.50)
90N(0.49)
891N(0.11)
822N-AT1h(0.71)
822N-AT6h(1.01)
822N-AT16h(1.44)
(b)
820H(0.48)
822H(0.54)
840H(0.15)
860H(0.46)
891H(0.12)
(c)
360N(1.17)
500N(0.74)
640N(0.51)
930N(0.47)

Figure 9

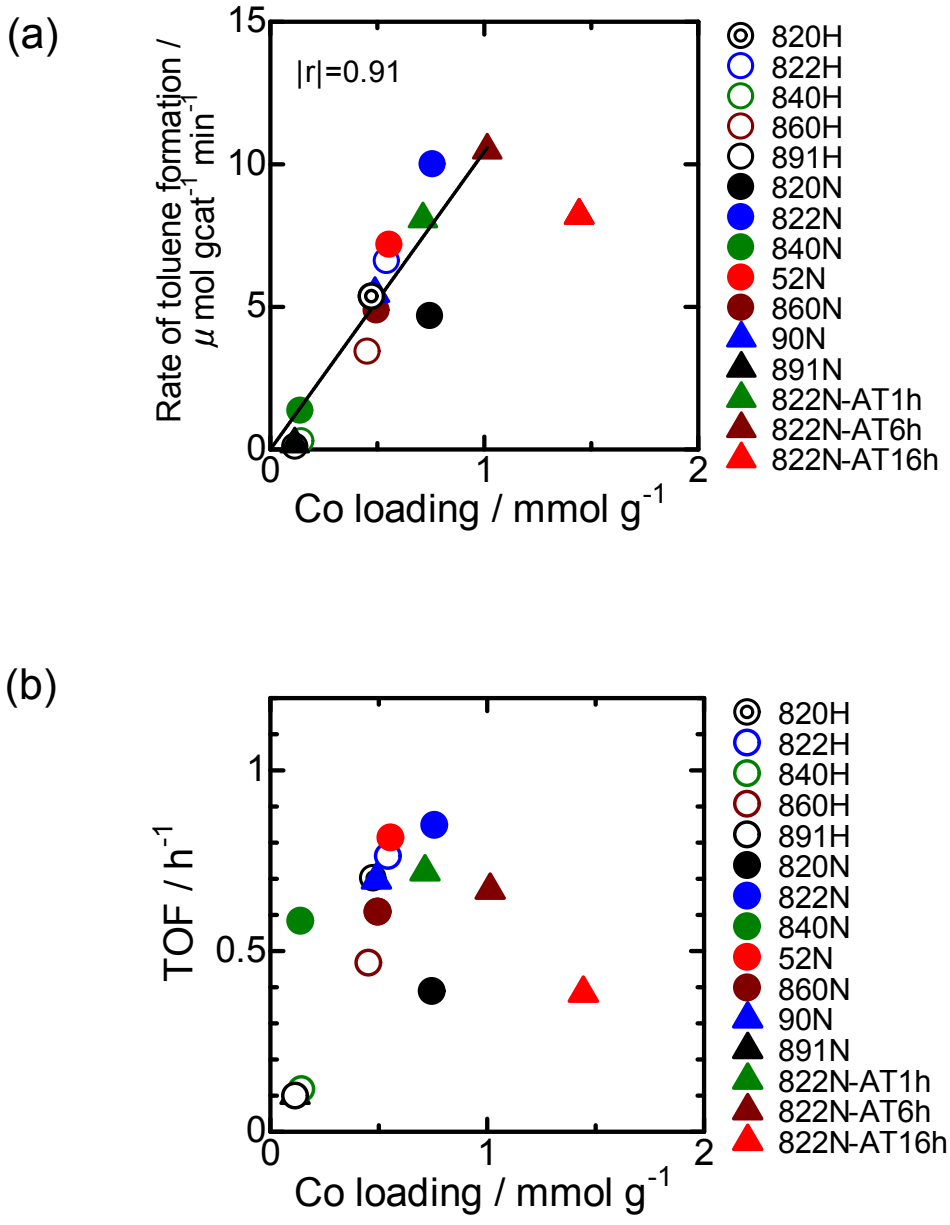
(a)
|r|=0.91
Rate of toluene formation / μ mol gcat-1 min-1
Co loading / mmol g-1
820H
822H
840H
860H
891H
820N
822N
840N
52N
860N
90N
891N
822N-AT1h
822N-AT6h
822N-AT16h
(b)
TOF / h-1
Co loading / mmol g-1
820H
822H
840H
860H
891H
820N
822N
840N
52N
860N
90N
891N
822N-AT1h
822N-AT6h
822N-AT16h

Figure 10